HOSTED BY
ELSEVIER
CrossMark
Available online at www.sciencedirect.com
ScienceDirect
Progress in Natural Science: Materials International 25 (2015) 460–470
Progress in Natural Science Materials International
www.elsevier.com/locate/pnsmi
www.sciencedirect.com

Original Research

Investigation on microstructural, mechanical and electrochemical properties of aluminum composites reinforced with graphene nanoplatelets

Muhammad Rashad[a,b,*], Fusheng Pan[a,b,c,*,1], Zhengwen Yu[a,b], Muhammad Asif[d], Han Lin[a,b], Rongjian Pan[a,b]

[a]College of Materials Science and Engineering, Chongqing University, Chongqing 400044, China
[b]National Engineering Research Center for Magnesium Alloys, Chongqing University, Chongqing 400044, China
[c]Chongqing Academy of Science and Technology, Chongqing 401123, China
[d]School of Materials Science and Engineering, Dalian University of Technology, Dalian 116024, China

Received 4 March 2015; accepted 20 June 2015
Available online 31 October 2015

Abstract

In present study, the microstructure, mechanical and electrochemical properties of aluminum–graphene nanoplatelets (GNPs) composites were investigated before and after extrusion. The contents of graphene nanoplatelets (GNPs) were varied from 0.25 to 1.0 wt.% in aluminum matrix. The composites were fabricated thorough powder metallurgy method, and the experimental results revealed that Al-0.25%GNPs composite showed better mechanical properties compared with pure Al, Al-0.50%GNPs and Al-0.1.0%GNPs composites. Before extrusion, the Al-0.25% GNPs composite showed ~13.5% improvement in ultimate tensile strength (UTS) and ~50% enhancement in failure strain over monolithic matrix. On the other hand, Al-0.50%GNPs and Al-0.1.0%GNPs composites showed the tensile strength lower than monolithic matrix. No significant change was observed in 0.2% yield strength (YS) of the composites. However, the extruded materials showed different trends. The 0.2%YS of composites increased with increase in GNPs filler weight fractions. Surprisingly, UTS of composites with 0.25 and 0.50% GNPs was lower than monolithic matrix. The failure strain of the baseline matrix was enhanced by ~46% with 0.25% graphene nanoplatelets. The superior mechanical properties (in terms of failure strain) of the Al-0.25%GNPs composite maybe attributed to 2-D structure, high surface area and curled nature of graphene. In addition, the corrosion resistance of pure Al and its composites reinforced with 0.5 and 1.0 wt% GNPs was also investigated. It was found that the corrosion rate increased considerably by the presence of GNPs.

Keywords: Aluminum–graphene composites; Powder metallurgy; Corrosion; Tensile property

1. Introduction

Graphene, single layer of sp^2 hybridized carbon atoms, has attracted a great attention to research owing to its unique electrical [1–5], thermal [6–8] and mechanical properties [9–13]. Graphene nanoplatelets (GNPs), few layer graphene sheets have high specific surface area, and hence it is qualified as a gorgeous material for fabricating composites with high mechanical properties. The low density of graphene, varying from 0.03 to 0.1 g/cc for GNPs, may lead to interesting weight lightening in polymers, ceramic or metal matrix composites (MMCs). Several researchers reported the GNPs reinforced polymer composites with improved mechanical properties [14–20]. Apart from polymer matrices, ceramic and metal matrices have also been used to fabricate GNP reinforced composites. Recently, Wang et al. [21] found that the addition of 2 wt% graphene nanosheets to Al_2O_3 matrix led to the increase in fracture toughness (+53%). In another work, Walker

*Corresponding authors at: College of Materials Science and Engineering, Chongqing University, Chongqing 400044, China. Tel.: +86 23 6511 2635; fax: +86 23 6730 0077.
E-mail addresses: rashadphy87@gmail.com (M. Rashad), fspan@cqu.edu.cn (F. Pan).
[1]+86 13594159131.
Peer review under responsibility of Chinese Materials Research Society.

http://dx.doi.org/10.1016/j.pnsc.2015.09.005

et al. [22] found that the fracture toughness of monolithic Si_3N_4 can be enhanced (+136%) with the addition of 1.5 vol% graphene platelets (GPLs). Similarly, GPLs were also used to enhance the fracture toughness of Si_3N_4 and ZTA in other reports [23,24].

According to up-to-date research, several attempts have been made to fabricate the metal matrix composites reinforced with graphene sheets, i.e. magnesium–GNPs [25–28], and copper–GNPs [29,30], via conventional powder metallurgy and stir casting techniques. However, so far, the reported studies were essentially limited to pure aluminum matrices [31–34]. S.F. Bartolucci and co-workers [31] fabricated a 0.1 wt% MLG/Al composite by applying high-energy ball milling, hot isostatic pressing (648 K), and hot extrusion (823 K) in sequence, however, the strength of the processed composite was less than that of the counterpart without graphene. Wang et al.[32] fabricated the 0.3 wt% MLG–Al composite through powder metallurgy method. The MLG–Al composite powders were consolidated by sintering in an argon atmosphere at 853 K followed by hot extrusion at 713 K. Recently, Pérez-Bustamante et al. [33] investigated the effect of milling time and sintering time on micro hardness of Al/GNPs composites. GNPs were added with 0.25, 0.50 and 1.0 wt% into an aluminum powder matrix. Milled powders were cold consolidated and subsequently sintered. In authors' previous work [34], it was demonstrated that the liquid state mixing of GNPs in aluminum powder was effective in fabricating Al/GNPs composites.

However, the influence of GNPs contents and extrusion on the mechanical properties of the Al/GNPs composites has been hardly reported so far. In the present work, Al matrix was reinforced with 0.25, 0.50 and 1.0 wt% GNPs. The mechanical properties of composites in as sintered and as extruded conditions were investigated and compared to pristine matrix. In addition, corrosion resistance of materials was examined in NaCl solution. The experimental results revealed that the mechanical properties of synthesized composites were improved by the addition of 0.25 wt% GNPs in the Al matrix.

2. Experimental procedures

2.1. Materials

The GNPs were synthesized using CVD by Nanjing Xian Feng Nano Material Technology Co. Ltd. Jiangsu, China. The GNPs were delivered as wrinkled, curled, overlapped stacks of graphene sheets as shown in Fig. 1(a). The GNPs consisted of platelets with the morphology of irregular shaped flakes with mean diameters less than 0.5–20 μm and agglomerated powders with opaque structure (Fig. 1(b)). The thickness of the GNPs was several nanometers (5–25 nm), corresponding to approximately 15–75 sheets of graphene (assuming that the thickness of monolayer graphene is 0.35 nm [35]). Fig. 1(c) shows the X-ray diffraction (XRD) analysis of as received GNPs. The matrix precursor was pure aluminum powder (99.5% in purity) with an average particle size of

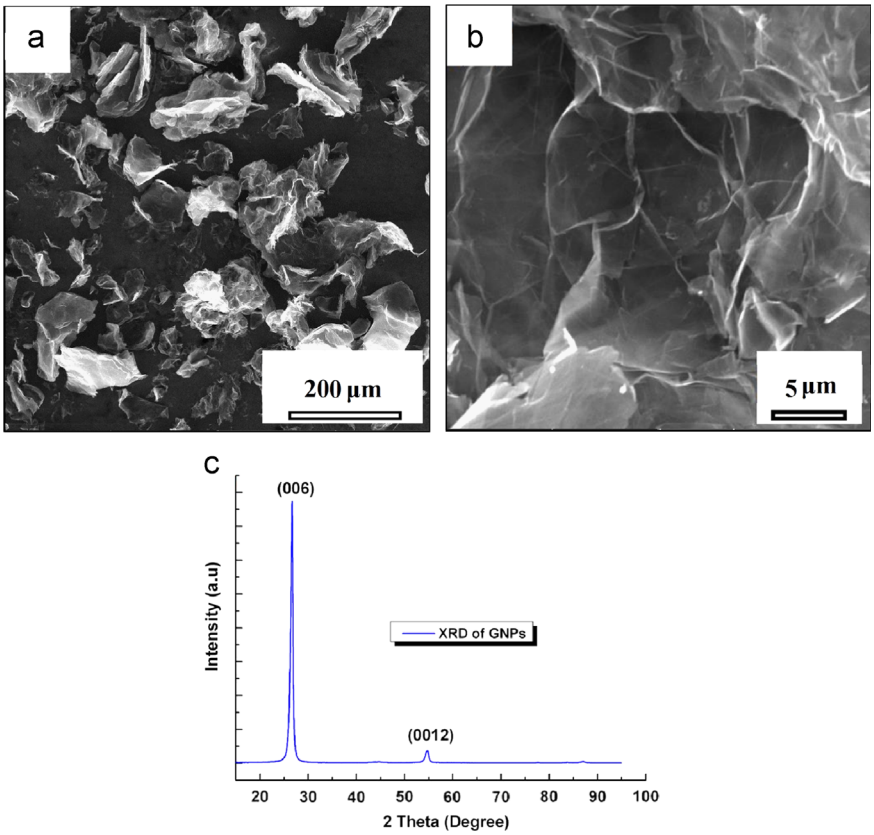

Fig. 1. SEM micrographs of GNPs at (a) low magnification; (b) high magnification; (c) XRD graph of as received GNPs.

about 2 μm. This metal exhibits good specific mechanical characteristics, good corrosion resistance and is widely used in the aerospace industry.

2.2. Fabrication of Al/GNPs composite powders

A simple strategy (solution based powder metallurgy method) was used to synthesize the GNPs/Al composites. In the first step, GNPs were ultra-sonicated separately in ethanol to achieve uniform dispersion. After ultra-sonication for about 1 h, GNPs dispersions was added drop wise into the Al slurry in ethanol. The mixture was stirred for 1 h using a mechanical agitator at 2000 RPM speed. After mechanical mixing the composite mixture was filtered and vacuum dried at 80 °C for 12 h to obtain Al/GNPs composite powder. The powder mixtures for different materials i.e. pure Al, Al/0.25 wt% GNPs, Al/0.50 wt%GNPs, and Al/1.0 wt%GNPs composites were prepared using above stated method.

2.3. Consolidation of Al/GNPs composite powders

Hot extrusion was used to consolidate the composite powders. Prior to extrusion, they were placed into a steel die and were compacted to a column ($\Phi 80 \times 20$ mm) under 540 MPa pressure, and then the column was sintered in flowing Ar atmosphere at 600 °C for 5.5 h. Finally, the column was heated to 470 °C with a heating rate of 10 °C/min within a vacuum furnace installed with the extruder. Extrusion was conducted with an extrusion ratio of 5:1 at a ram speed of 1.0 mm/min. The final diameter of the extruded rods was 16 mm and there was no crack appearing on the surface of the rods.

2.4. Properties characterization

Raman spectroscopy was used to characterize as received GNPs and mechanically agitated composite powders. Raman spectrometer (Renishaw inVia plus, Renishaw, Gloucestershire, UK), with excitation laser of 632 nm wavelength and 50x objective lens was used to evaluate the thickness of as received GNPs and its quality in composite powders. Samples for microstructure characterization were polished using different grades of emery papers followed by etching in acidic solution.

X-ray diffraction analysis on polished extruded sample bars were carried out by X-ray diffraction (D/MAX-1200, China), using Cu Kα radiation for 20–90° range. Raw XRD data were refined and analyzed via MDI Jade 6.0 program (Materials Data Incorporated: Livermore, CA, USA).

Scanning electron microscopy equipped with energy-dispersive spectrometer (EDS) was used to analyze the surface morphology. Transmission electron microscopy (TEM) was used to investigate the interface between matrix and reinforcements. The corrosion resistance of pure Al and composites reinforced with 0.5 and 1.0 wt% GNPs was studied in 3.5 wt% NaCl solution using evolved potentiodynamic polarization measurement. All the electrochemical experiments were recorded after the electrode immersion in the test solution for 25 min before measurements. Microstructure and morphology of the corroded surfaces were analyzed using scanning electron microscopy (SEM). The densities of developed materials were analyzed using electronic density meter with accuracy of 0.1 mg. The samples were weighted in air, then dipped in distilled water, and the densities of the samples were calculated according to Archimedes' principle. Three samples were made for each composition to minimize the error. The theoretical densities of materials were calculated by the rules of mixture. The density of aluminum and GNPs was 2.7 and 2.23 g/cm^3 respectively.

The Vickers hardness of samples was tested under a load of 100 g with dwell time of 15 s. To evaluate the mechanical properties, tensile tests were conducted at room temperature with an initial strain rate of 1×10^{-3} s $^{-1}$ using a tensile test machine (R&B UNITECH™). Tensile specimens with a gauge length of 15 mm, a gauge diameter of 5 mm were machined from as sintered and as extruded samples using the electro-discharge machining process. Images of tensile fracture surfaces were taken using SEM.

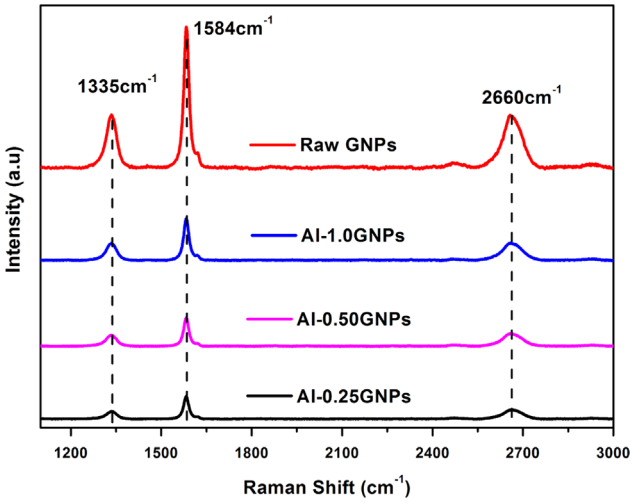

Fig. 2. Raman spectra of as received Graphene nanoplatelets and mechanical agitated composite powders.

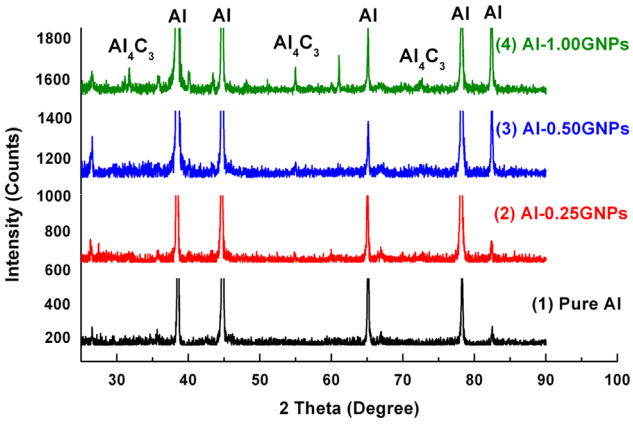

Fig. 3. X-ray diffraction of pure aluminum and its composites in extruded condition.

3. Results and discussion

3.1. Raman spectroscopy

Raman spectroscopy is a fast technique to provide a direct insight on electro-phonon interactions, which implies a high sensitivity to electronic and crystallographic structures [35,36]. Raman spectra of carbon materials possess three main bands between 1200 and 2800 cm^{-1} region. D band at $\sim$1360 cm^{-1} is due to out of plane breathing mode of sp^2 atoms [37]. It attributes to disorder of graphitic base materials due to presence of impurities. G band at around 1580 cm^{-1} corresponds to the E_{2g} phonon at the center of Brillion zone. 2D band at around 2700 cm^{-1} is a major fingerprint of graphene. The shape, position and intensity relative to G band of this peak depend on number of layers [38]. Fig. 2 illustrates Raman spectra of as received GNPs and mechanically agitated composite powders. The Raman spectra reveal the presence of D, G and 2D peaks. Raman Spectra of GNPs and mechanically agitated composite powders dispersed on SiO_2

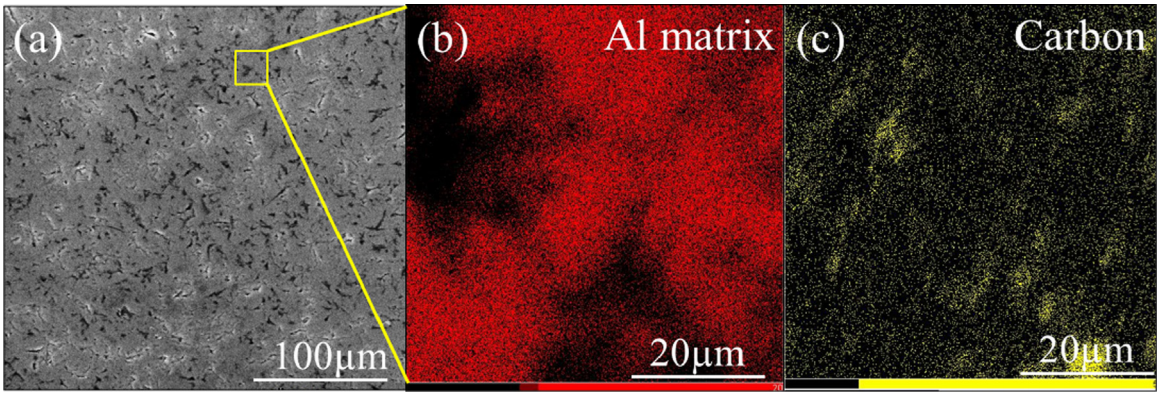

Fig. 4. X-ray mapping of Al-1.0GNP composite showing the existence of carbon.

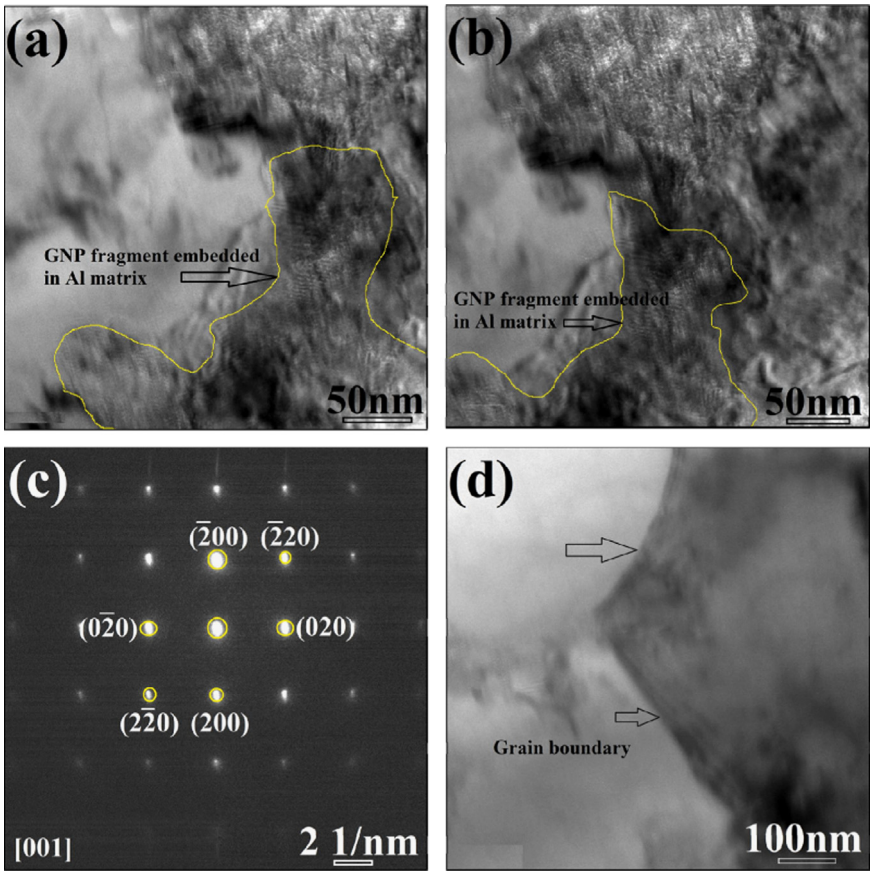

Fig. 5. TEM images of Al-0.25GNPs composite where GNP fragment is embedded in Al matrix with good interfacial adhesion (a,b); (c) Selected Area Diffraction pattern; (d) TEM image showing grain boundary.

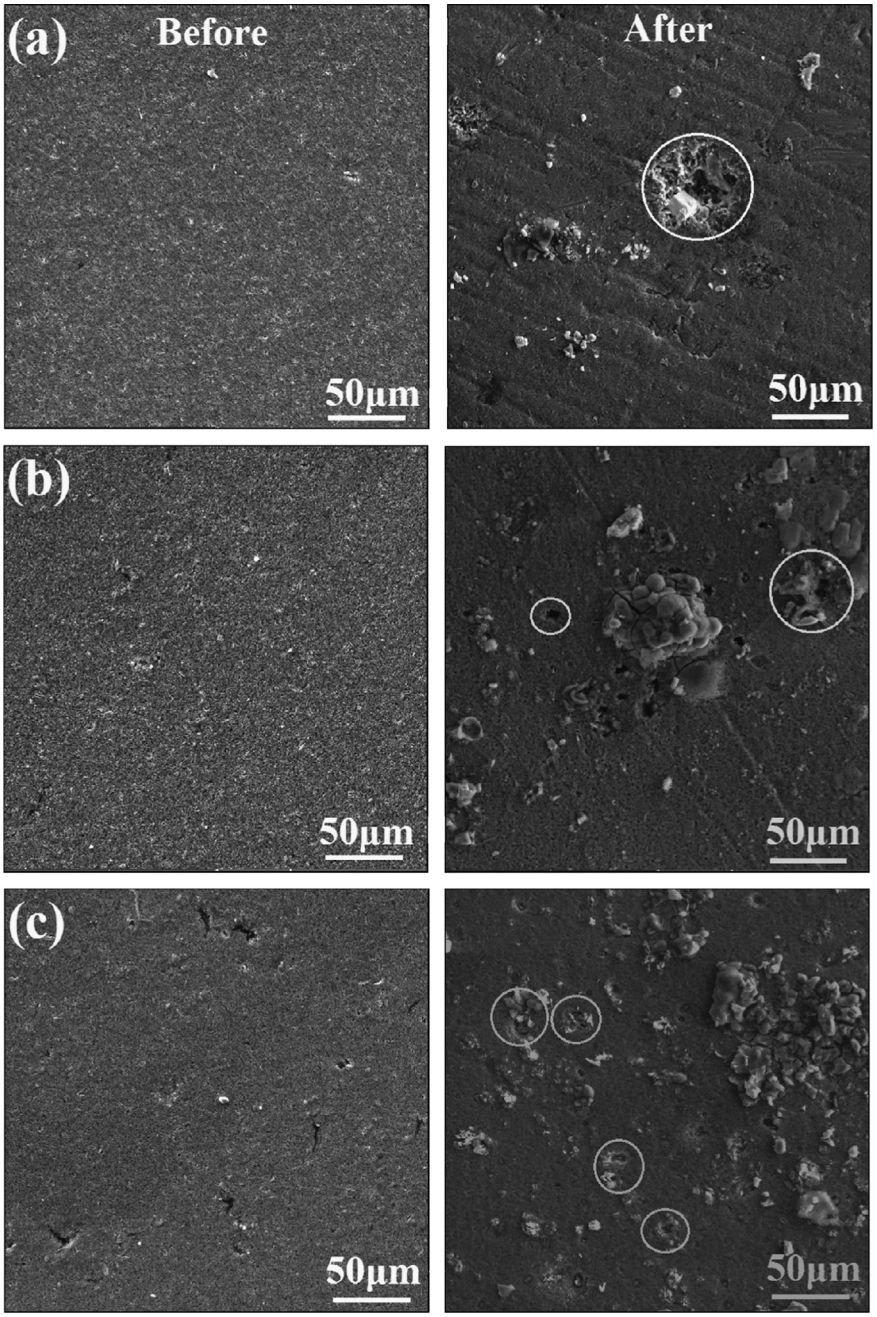

Fig. 6. SEM micrographs of sintered Al and its composites before and after corrosion tests: (a) Pure Al, (b) Al-0.5GNPs, (c) Al-1.0GNPs.

substrate exhibited a significant D band at 1335 cm^{-1}, strong G band at 1584 cm^{-1} and a broad second order 2D band at 2660 cm^{-1}. Intensity of D, G and 2D bands in mechanically agitated composite powders was very low, which may be attributed to the low content of GNPs in composite powders. Existences of these peaks confirm that GNPs were not damaged during mechanical agitation process.

3.2. X-ray diffraction

Fig. 3 shows X-ray diffraction patterns from the pure Al and its composites in the extruded condition. Reflections attained to the carbon element were not presented. This is attributed to the nanometric size and the low content of the reinforcement phase, which cannot be detected due to the detection limit presented by XRD for second phases [39]. It can be observed that the effect of chemical reaction between GNPs and Al matrix may results in the formation of a compound, identified as the aluminum carbide Al_4C_3. The presence of aluminum carbide has been observed in the production of CNT/Al composites synthesized by several routes, where its formation shows a strong dependence on the processing temperature in the production of the composites [40]. This observation agrees with the results obtained by Bartolucci et al. [31], where they reported the formation of aluminum carbide in graphene–aluminum composites processed by hot extrusion.

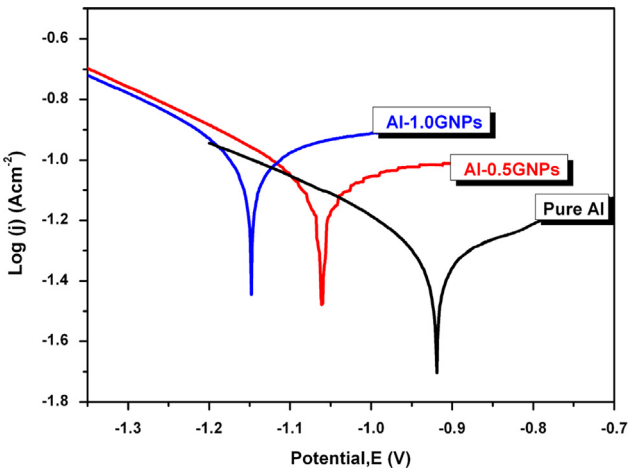

Fig. 7. Potentiodynamic polarization curves for Pure Al and its composite samples in 3.5 wt% NaCl solution.

Table 1
E_{corr} and j_{corr} values of pure Al and its composites in 3.5 wt% NaCl solution.

Sample	E_{corr}(V vs. Ag/AgCl)	j_{corr} (μA cm^{-2})
Al	−0.9188	0.031
Al-0.5 wt%GNPs	−1.0613	0.976
Al-1.0 wt%GNPs	−1.1478	2.561

Table 2
Theoretical/experimental densities and Vickers hardness of materials in as sintered and as extruded conditions.

Materials	Conditions	Theoretical density(g/cm^3)	Measured density(g/cm^3)	Vickers hardness (Hv)
Pure Al	Before	2.7000	2.6996	69
Al-0.25GNPs	Extrusion	2.6991	2.6986	71
Al-0.50GNPs		2.6976	2.6961	74
Al-1.00GNPs		2.6943	2.6901	77
Pure Al	After	2.7000	2.6991	76
Al-0.25GNPs	Extrusion	2.6991	2.6980	80
Al-0.50GNPs		2.6976	2.6962	85
Al-1.00GNPs		2.6943	2.6911	90

3.3. Microstructure characterization

In order to confirm the existence and dispersion of GNPs in aluminum matrix, X-ray mapping was carried out on Al-1.0GNPs composite surface using energy-dispersive spectroscopy as shown in Fig. 4(a)–(c). It can be seen from Fig. 4 (a) that the thick stacks of GNPs were embedded in Al matrix. These GNPs stacking may be due to pi–pi interactions between different graphene sheets and may adversely affect the mechanical strength of the composite.

Fig. 5(a)–(d) present the TEM images of the Al-0.25GNPs composite. Platelet-like GNP fragments with widths of 50–150 nm and lengths of 100–200 nm were embedded in the Al matrix, were frequently encountered as shown in Fig. 5(a) and (b). The GNP particles and fragments embedded in matrix results in the efficient load to transfer from matrix to reinforcements. In addition, due to the difference in the thermal expansion coefficients between graphene and aluminum ($\alpha_{graphene}=0.9\times10^{-6}$/K at 873–1073 K [41–43] and $\alpha_{Al}=23.6\times10^{-6}$/K), dislocations are generated, which lead to increased strength of composite when their motion is resisted by reinforcement particle. Fig. 6(c) and (d) show the SAD pattern and grain boundary in the composite matrix.

3.4. Electrochemical measurements

One of the main obstacles to the use of aluminum composites is the influence of reinforcement on corrosion resistance. This is particularly important for aluminum based composites, where a protective oxide film imparts the corrosion resistance. The addition of a reinforcing phase could lead to further discontinuities in the film, increasing the number of sites where corrosion can be initiated and rendering the composite liable to severe attack [44]. The effect of reinforcements (GNPs) on corrosion resistance of pure aluminum was investigated.

Microstructures of pure Al and Al–GNPs composites before and after corrosion tests are shown in Fig. 6. It can be seen that the surfaces of samples before corrosion tests are very clear. However, after corrosion test the surface was corroded and no longer clear. Several pits were evident on the surface, and the compound that may be found on the surface was mainly aluminum oxide with the traces of sodium chloride salt.

Corrosion potential (E_{corr}) and corrosion current density (j_{corr}) are often used to characterize the corrosion resistance of test specimens. In general, high corrosion potential and low corrosion current density suggest good corrosion resistance. The potentiodynamic polarization curves of the pure Al and Al–GNPs composite specimens in 3.5 wt% NaCl solution are depicted in Fig. 7. The corresponding E_{corr}, j_{corr} and corrosion rate(**CR**) of the specimens have been derived and listed in Table 1.

It can be seen that the E_{corr} of pure Al is higher than that of Al–GNPs composites, and the j_{corr} values of pure Al are much lower than that of composites, which means that the pure Al specimen has a higher corrosion resistance. On the other hand, the Al–GNPs composites exhibited low E_{corr} and higher j_{corr} values than that of the pure Al specimen, which means that Al–GNPs composite specimens have lower corrosion resistance. The corrosion resistance decreased with increasing GNPs contents, which is consistent with previous study [45]. According to Saxena et al. [46], the higher corrosion rate of Al–GNPs composite than the aluminum itself is possibly due to the graphene particles being cathodic relative to the matrix, thus leading to galvanic corrosion in the presence of an electrolyte [47]. It is generally agreed that the cathodic reaction for Al is believed to be the oxygen reduction as follows [48,49];

$$O_2+2H_2O+4e^-\rightarrow 4OH^- \quad (1)$$

Further increasing the potential towards the positive direction leads to rapid increase of the current in the anodic reaction

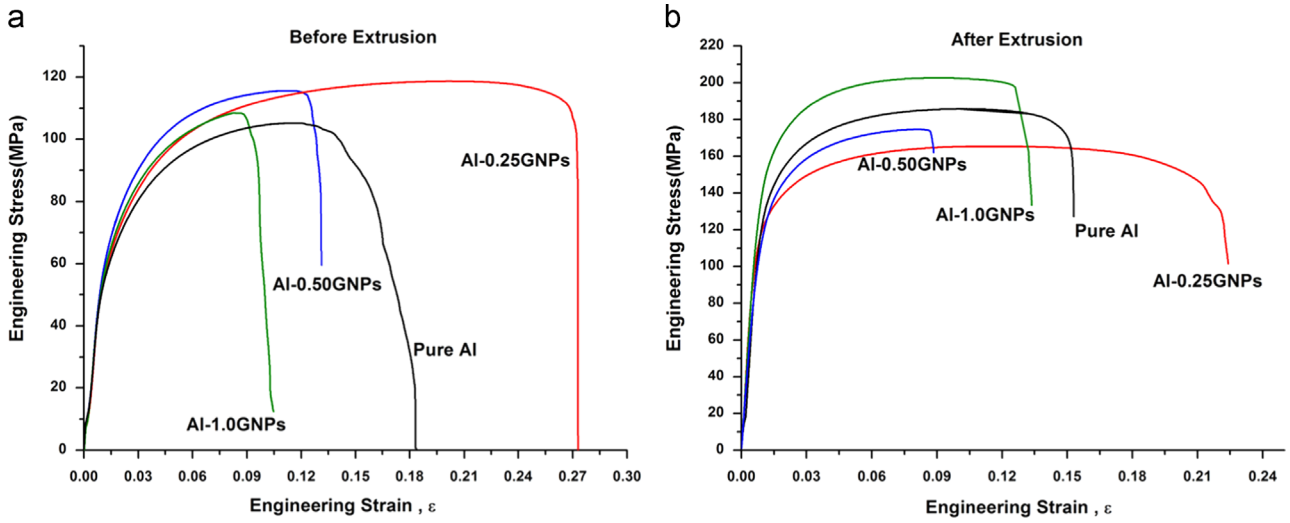

Fig. 8. Room temperature tensile stress–strain curves of pure Al and its composites before and after extrusion.

Table 3
Room temperature tensile properties of pure Al and its composites.

Sample	Before Extrusion			After Extrusion		
	0.2%YS (MPa)	UTS (MPa)	FS (%)	0.2%YS (MPa)	UTS (MPa)	FS(%)
Pure Al	57	105	18	112	186	15
Al-0.25GNPs	58	119	27	117	166	22
Al-0.50GNPs	64	116	13	120	175	08
Al-1.00GNPs	59	108	10	145	203	13

YS: Yield strength; UTS: Ultimate tensile strength; FS: Failure strain.

due to the dissolution of aluminum metal, Al (0), into aluminum cations, Al (III), with the release of electrons according to the following reactions [49]:

$$Al \rightarrow Al^{3+} + 3e^{-} \quad (2)$$

After the rapid increases of current, the polarization curve shows a large passivation region, which is most probably due to the formation of an oxide film and/or a corrosion product layer on the surface of Al and its composites. This is due to the reaction of Al^{3+} (Eq.(3)) with hydroxide ions from the solution to form an adsorbed layer of aluminum hydroxide on the surface:

$$Al^{3+} + 3OH^{-} \rightarrow Al(OH)_{3,ads} + 3e^{-} \quad (3)$$

The formed $Al(OH)_{3,ads}$ further transforms to aluminum oxide via the following reaction:

$$Al(OH)_{3,ads} \rightarrow Al_2O_3 + H_2O \quad (4)$$

The formation of such oxide greatly protects the surface against corrosion until the potential reaches the breakdown value at which the current abruptly increases as a result of the breakdown of the passive layer and the occurrence of pitting corrosion [48,49]. The breakdown of the passive oxide film also allows the aluminum surface to be attacked by the aggressive ions presented in the solution, i.e. chlorides, to form aluminum chloride complex, $AlCl_4$, as can be expressed by the following reaction:

$$Al^{3+} + 4Cl^{-} \rightarrow AlCl_4^{-} \quad (5)$$

It has been reported [50,51] that a salt barrier of $AlCl_3$ formed within the pits on their formation, which could then form $AlCl^{4-}$ (Eq. (6)), and diffused into the bulk of the solution. On the other hand, it has been proposed [52] that the chloride ions do not enter into the oxide film, but they are chemisorbed onto the oxide surface and act as a reaction partner, aiding the oxide to dissolve via the formation of oxychloride complexes.

$$Al^{3+} + 2Cl^{-} + 2OH^{-} \rightarrow Al(OH)_2Cl_2^{-} \quad (6)$$

3.5. Density analysis and Vickers hardness

Theoretical and experimental densities of pure aluminum and its composites are summarized in Table 2. Theoretical and experimental density calculations revealed the decrease in composites densities with increasing reinforcements (GNPs) contents. This may be attributed to the low density (2.23 g/cm^3) of GNPs. The experimental densities are slightly lower than theoretical values, since at high sintering temperature the diffusion between the matrix and reinforcement particle is easier, which results in better sinterability of materials. Additionally, no significant difference in experimental densities was observed before and after extrusion, which may be attributed to the low extrusion ratio (5:1).

The Vickers hardness results of pure aluminum and its composites are summarized in Table 2. It can be observed that the hardness values increases with increase in GNPs weight contents in aluminum matrix. The increased hardness of composite materials may be due to presence of reinforcement particles possessing high strength and offer high constraint during indentations. Furthermore, the hardness of pure aluminum and its composites increased after extrusion process. It may be concluded that the extrusion process play vital role by

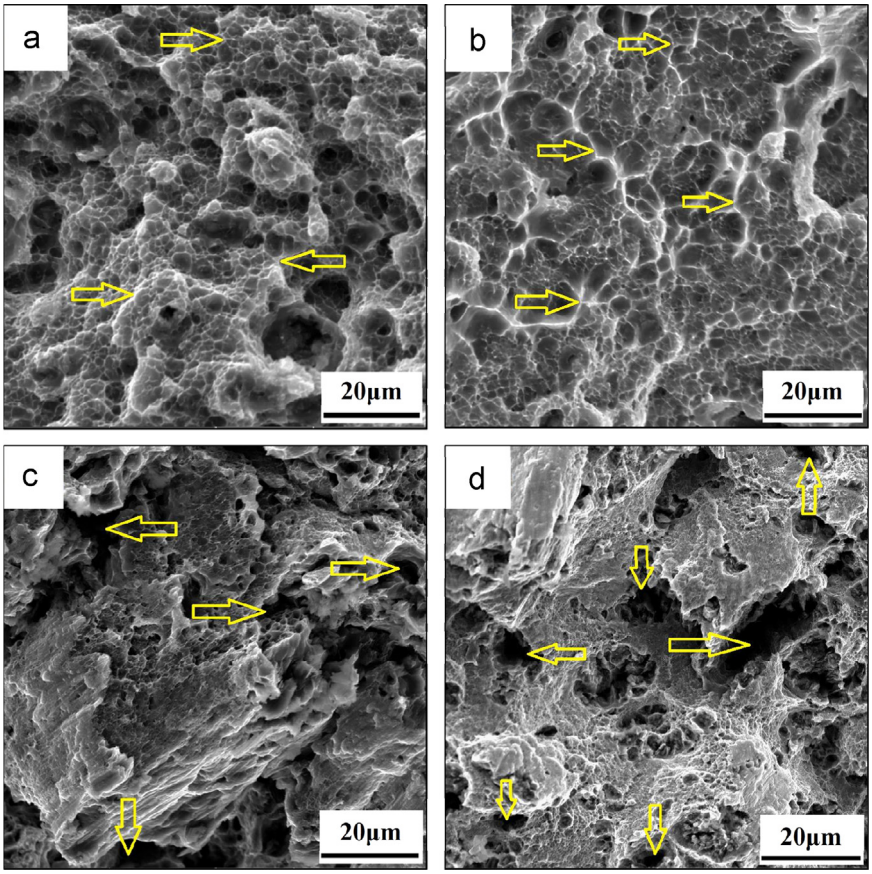

Fig. 9. Tensile fracture images of (a) Pure Al; (b) Al-0.25GNPs; (c) Al-0.50GNPs; (d) Al-1.0GNPs composites.

minimizing the voids and cavities in sintered materials, therefore led to increase in mechanical properties of composites

3.6. Tensile properties

The stress-true strain curves of the materials at room temperature before and after extrusion are presented in Fig. 8 (a) and (b), respectively. The average values of the yield stress (YS), ultimate tensile strength (UTS), and failure strain (%) measured from the engineering stress-engineering strain curves are provided in Table 3. The effect of the addition of 0.25 wt% GNPs on tensile properties was large in as-sintered condition because the low content of GNPs could disperse in aluminum matrix easily without overlapping and coagulation. There was a significant increase of the UTS and FS with the addition of 0.25 wt%GNPs in Al matrix. In contrast, the effect of large content (0.50 wt% and 1.0 wt%) of GNPs on tensile properties was adverse. Both tensile strength and failure strain decreased with the increase in GNPs additions. This may be due to overlapping of GNPs with each other and due to strong pi–pi attractions between graphene sheets. The tensile properties of composites in as-extruded condition are surprising. The addition of 0.25 wt% GNPs into pure Al led to the increase in failure strain, however the YS and UTS were decreased. When GNPs content reached 1.0 wt% in Al matrix, both YS and UTS values increased with a reduction in failure strain. From the results and analysis above, it may be concluded that low GNPs (0.25%) outperform high GNPs (0.50,1.0%) additives in aluminum matrix. Such improvement in mechanical behavior of composites is attributed to the high strength and excellent adhesion of GNPs with matrix particles, which resist against rupture during tensile loading. As a result GNPs and Al_4C_3 phase resist the dislocation motion across the matrix-reinforcement interface [53].

The mechanical properties of aluminum [32] and magnesium [25] metal composites also improved with addition of graphene nanoplatelets in previous studies. However, the elongations of resulting composites were adversely affected. Similarly in present work, when GNPs content exceeds 0.25 wt% (in aluminum matrix) the tensile strength increased, but elongation reduced as shown in Table 3 and Fig. 8. The reduction in elongation or failure strain values of composites may be attributed to stacking of GNPs to form thick graphite particles, which is caused by pi–pi attractions between graphene layers as shown in Fig. 4.

Load transfer from matrix to reinforcement can be explained using a Shear lag model. Load transfer from matrix to reinforcement depends largely on interfacial bonding between the matrix and the reinforcement by interfacial shear stress [54,55]. In case of metal matrix composites there are four kind of interfacial bonding, i.e (a) mechanical bonding, (b) van der Waals attractions, (c) diffusion bonding, and (d) reaction bonding [56]. In present case, adhesion of GNPs (due to its wrinkled surface) with Al matrix is named as mechanical

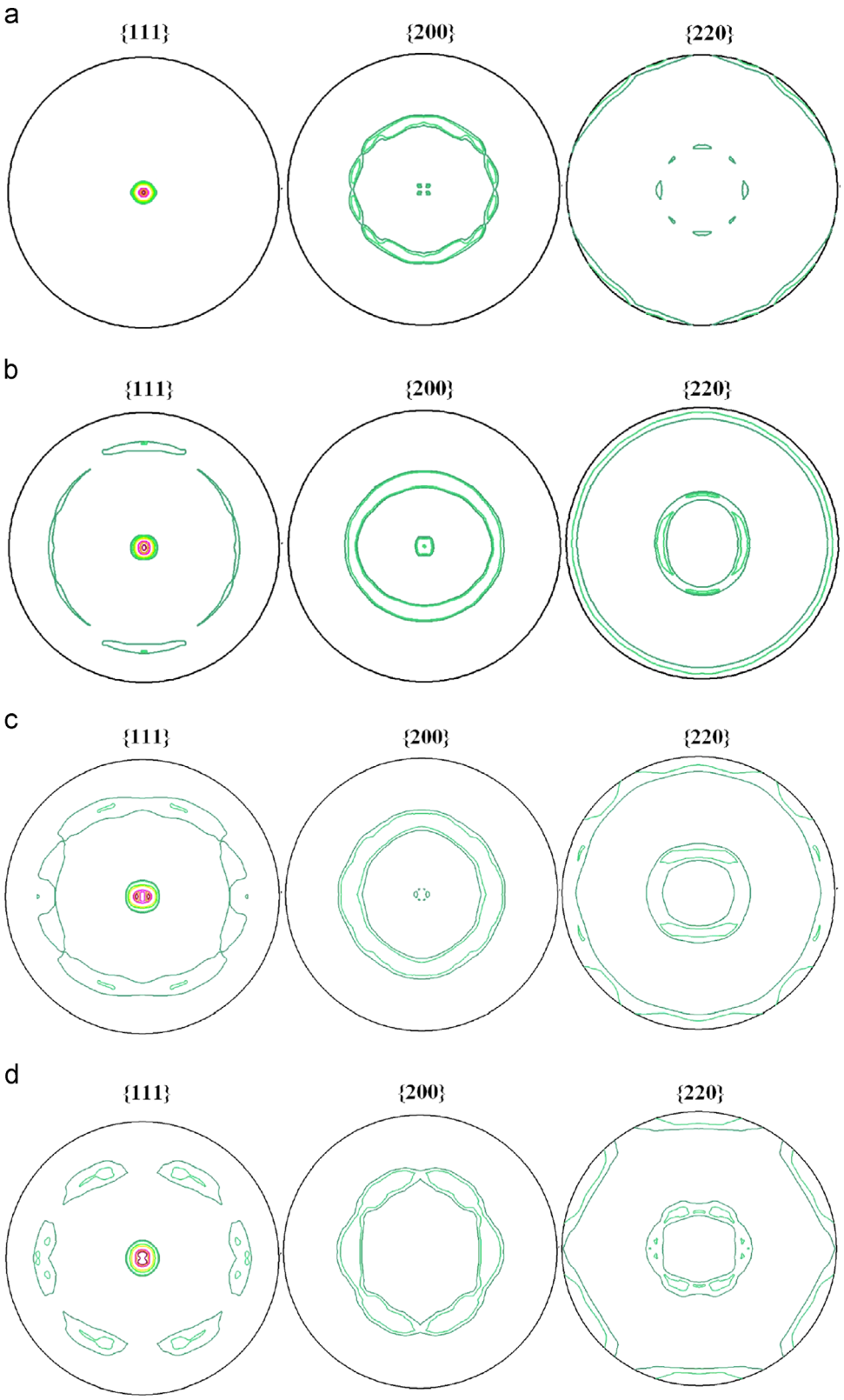

Fig. 10. Pole figures {111}, {200}, {220} of (a) Pure Al; (b) Al-0.25GNPs; (c) Al-0.50GNPs; (d) Al-1.0GNPs composites.

bonding. This bonding is dominant over van der Waals attractions in Al-0.25GNPs composites, thus results in high failure strain values of composite caused by efficient load transfer from soft matrix to hard GNPs. On the other hand, van der Waals attractions are dominant over mechanical bonding in Al-0.5GNP and Al-1.0GNP composites, thus stacking of GNPs may lead to reduced failure strain values. In addition, GNPs enhances the strength of matrix when they aligned

Table 4
Crystallographic texture results of pure aluminum and its composites taken perpendicular to the extursion direction

Samples	Pole figures	I/I_{max}
Pure Al	{111}	0.90
	{200}	0.18
	{220}	0.18
Al-0.25GNPs	{111}	0.91
	{200}	0.19
	{220}	0.19
Al-0.50GNPs	{111}	0.92
	{200}	0.25
	{220}	0.25
Al-1.0GNPs	{111}	0.94
	{200}	0.32
	{220}	0.32

I_{max} is the XRD maximum intensity from pole figures {111}, {200} or {220}.

parallels to tensile direction since GNPs has high strength in-plane direction. This is because of its two dimensional structure and large specific surface area [57].

It can be observed that overall tensile strength of composite is just 203 MPa. The low improvement in tensile strength of composites may be attributed to following reasons. Stacking of GNPs at high weight fractions is a big challenge due to pi–pi forces between graphene layers. In addition, since the used GNPs are multilayer graphene their strength is very low compared to single layer graphene. Orientation of GNPs in the composite matrix is also an important factor to strongly influence the strength of resulting material. The GNPs aligned along the tensile direction have positive influence on tensile strength due to the efficient load transfer between reinforcement and matrix. Load transfer depends on adhesion of GNPs with matrix particles. Several techniques can be used to improve these technical weaknesses. Ball milling can be used to disperse GNPs in matrix with good interfacial adhesion. This can improve the dispersion of GNPs along with good cold bonding between reinforcements and matrix. And therefore the tensile strength of composite may be improved. Another way to overcome these problems is chemical functionalization of graphene with some organic polymers i.e polyvinyl alcohol, which may help to improve the matrix-reinforcement bodings [58,59].

3.7. Fracture surface analysis

Fig. 9 shows the SEM images of the tensile fracture surfaces of as-extruded pure Al and its composite. As shown in Fig. 9, the plastic deformation, represented by the ductile fracture dimples, decreased as GNPs content increased. Comparing the pure Al (Fig. 9(a) and (b)) and the Al-0.25 wt%GNP composite, a change in the morphology of the surface can be observed. The Al-0.25 wt%GNP composite contains more ductile fracture dimples than pure Al. In addition, no voids and cavities were observed in Al-0.25 wt%GNP composite. Therefore, Al-0.25 wt%GNP composite exhibited the highest value of failure strain among all composites. The dimples of the ductile fracture observed in the Al-0.50 wt%GNP and Al-1.0 wt%GNP composite samples diminished, and numerous cavities and voids were detected on sample fracture surfaces. As the GNPs content increased, the sharp decrease in the size of the ductile dimples of the fracture surface indicated that the ductility of the composite decreased significantly. This change in the fracture surface was also accompanied by a change in the mechanical behavior as discussed and shown in Fig. 8. As discussed earlier, 0.50 wt% and 1.0 wt% of GNPs are too much and were not convenient to be uniformly dispersed throughout the Al matrix, resulting in no enhancement in, or even deterioration of the mechanical properties.

3.8. Crystallographic texture measurements

Crystallographic texture measurements were carried out using diffractometer with Cu-Karadiation at 40 KV and 34 mA. The Pole figures {111}, {200} and {220} of pure Al and its composites, taken from the directions perpendicular to the extrusion, are shown in Fig. 10(a)–(d) and Table 4. Enhancement in tensile properties occurred due to the crystallographic texture difference between pure Al and Al–GNPs composites. The pole figure {111} of the pure Al sample confirmed the change in texture symmetry with the addition of GNPs particles. The pole intensity was concentrated at the center. However the addition of GNPs led to scattering of texture intensity towards the periphery of pole figure {111}. The change in the polar density distribution in the poll figures indicates that usual crystallization processes took place during sintering in the furnace. No significant change was observed in pole figure {200} of pure Al with the addition of GNPs particles. However, the pole figure {220} of the pure Al showed small amount of texture intensity at the center and along the periphery of pole figure. The addition of GNPs particles leads to increase in texture intensity, concentration at the center and along the periphery [60–63] as shown in Table 4.

4. Conclusions

In this study, the Al–Graphene nanoplatelets composites were fabricated by liquid state mixing of Al and GNPs, followed by pre-compaction at room temperature, sintering, and finally by hot extrusion. The microstructure was analzsed, the mechanical and electrochemical properties were tested for pure Al and Al–Graphene nanoplatelets composites in as-sintered and as-extruded states. Experimental results revealed that for both the as-sintered and as-extruded state, low GNPs (0.25%) outperform high GNPs (0.50,1.0%) additives in aluminum matrix. This may be due to the uniform dispersion of GNPs at low filling level in the composite matrix. The increased strength of composites is attributed to the basic strengthening mechanisms including Orowan looping, dislocation density generation, load transfer and crystallographic texture differences between pure Al and composites. The electrochemical results revealed that the corrosion rate increases considerably by the presence of GNPs. The

preliminary results suggest that the GNPs act as the effective cathodes to accelerate the corrosion.

Acknowledgment

The present work was supported by the National Natural Science Foundation of China (No. 50725413), the Ministry of Science and Technology of China (MOST) (Nos. 2010DFR50010 and 2011FU125Z07), and Chongqing Science and Technology Commission, Chongqing People's Municipal Government (CSTC2013JCYJC60001).

References

[1] A.K. Geim, K.S. Novoselov, Nat. Mater. 6 (3) (2007) 183.
[2] X. Lin, X. Liu, J. Jia, X. Shen, J.-K. Kim, Compos. Sci. Technol. 100 (0) (2014) 166.
[3] H. Shi, D. Shi, C. Li, S. Luan, J. Yin, Li RKY, Mater. Lett. 133 (0) (2014) 200.
[4] E. Zaminpayma, P. Nayebi, Phys. B: Condens. Matter 459 (0) (2015) 29.
[5] M. Asif, T. Yi, L. Pan, L. Jiayan, M. Rashad, M. Usman, J. Phys. Chem. C (2015).
[6] Z. Fan, A. Marconnet, S.T. Nguyen, C.Y.H. Lim, H.M. Duong, Int. J. Heat Mass Transf. 76 (0) (2014) 122.
[7] L. Gan, S. Shang, C.W.M. Yuen, S.-x Jiang, N.M. Luo, Compos. Part B: Eng. 69 (0) (2015) 237.
[8] M. Tian, L. Qu, X. Zhang, K. Zhang, S. Zhu, X. Guo, et al., Carbohydr. Polym. 111 (0) (2014) 456.
[9] Y. Lei, J. Sun, X. Gong, Phys. B: Condens. Matter 461 (0) (2015) 61.
[10] P.H. Shah, R.C. Batra, Comput. Mater. Sci. 95 (0) (2014) 637.
[11] V. Vijayaraghavan, A. Garg, C.H. Wong, K. Tai, S.S. Mahapatra, Measurement 50 (0) (2014) 50.
[12] C. Wang, Q. Peng, J. Wu, X. He, L. Tong, Q. Luo, et al., Carbon 80 (0) (2014) 279.
[13] Y.Y. Zhang, C.M. Wang, Y. Cheng, Y. Xiang, Carbon 49 (13) (2011) 4511.
[14] N. Hong, J. Zhan, X. Wang, A.A. Stec, T. Richard Hull, H. Ge, et al., Compos. Part A: Appl. Sci. Manuf. 64 (0) (2014) 203.
[15] K. Hu, D.D. Kulkarni, I. Choi, V.V. Tsukruk, Prog. Polym. Sci. 39 (11) (2014) 1934.
[16] T. Kuilla, S. Bhadra, D. Yao, N.H. Kim, S. Bose, J.H. Lee, Prog. Polym. Sci. 35 (11) (2010) 1350.
[17] J. Ma, Q. Meng, I. Zaman, S. Zhu, A. Michelmore, N. Kawashima, et al., Compos. Sci. Technol. 91 (0) (2014) 82.
[18] S.H. Ryu, A.M. Shanmugharaj, Chem. Eng. J.. 244 (0) (2014) 552.
[19] D.S. Yu, T. Kuila, N.H. Kim, J.H. Lee, Chem. Eng. J. 245 (0) (2014) 311.
[20] J. Zhang, D. Jiang, Carbon 67 (0) (2014) 784.
[21] K. Wang, Y. Wang, Z. Fan, J. Yan, T. Wei, Mater. Res. Bull. 46 (2011) 315.
[22] L.S. Walker, V.R. Marotto, M.A. Rafiee, N. Koratkar, E.L. Corral, ACS Nano 5 (2011) 3182.
[23] L. Kvetková, A. Duszová, P. Hvizdoš, J. Dusza, P. Kun, C. Balázsi, Scr. Mater. 66 (2012) 793.
[24] J. Liu, H. Yan, M.J. Reece, K. Jiang, J. Eur. Ceram. Soc. 32 (2012) 4185.
[25] L.-Y. Chen, H. Konishi, A. Fehrenbacher, C. Ma, J.-Q. Xu, H. Choi, H.-F. Xu, F.E. Pfefferkorn, X.-C. Li, Scr. Mater. 67 (2012) 29.
[26] M. Rashad, F. Pan, A. Tang, Y. Lu, M. Asif, S. Hussain, J. She, J. Gou, J. Mao, J. Magnes. Alloy. 1 (2013) 242.
[27] M. Rashad, F. Pan, M. Asif, A. Tang, J. Ind. Eng. Chem. 20 (2014) 4250.
[28] M. Rashad, F. Pan, A. Tang, M. Asif, M. Aamir, J. Alloy. Compd. 603 (2014) 111.
[29] W.J. Kim, T.J. Lee, S.H. Han, Carbon 69 (2014) 55.
[30] M. Rashad, F. Pan, A. Tang, M. Asif, J. She, J. Gou, J. Mao, H. Hu, J. Compos. Mater. 49 (2015) 285.
[31] S.F. Bartolucci, J. Paras, M.A. Rafiee, J. Rafiee, S. Lee, D. Kapoor, N. Koratkar, Mater. Sci. Eng. A 528 (2011) 7933.
[32] J. Wang, Z. Li, G. Fan, H. Pan, Z. Chen, D. Zhang, Scr. Mater. 66 (2012) 594.
[33] R. Pérez-Bustamante, D. Bolaños-Morales, J. Bonilla-Martínez, I. Estrada-Guel, R. Martínez-Sánchez, J. Alloy. Compd.
[34] M. Rashad, F. Pan, A. Tang, M. Asif, Prog. Nat. Sci. Mater. Int. 24 (2014) 101.
[35] W. Choi, I. Lahiri, R. Seelaboyina, Y.S. Kang, Crit. Rev. Solid State Mater. Sci. 35 (2010) 52.
[36] Ferrari A.C. MJ, V. Scardaci, C. Casiraghi, M. Lazzeri, F. Mauri, S. Piscanec, D. Jiang, K.S. Novoselov, S. Roth, A.K. Geim, Phys. Rev. Lett. 97 (2006) 187401.
[37] A.C. Ferrari JR, Phys. Rev. B 64 (2001) 075414.
[38] I. Calizo, A.A. Balandin, W. Bao, F. Miao, C.N. Lau, Nano Lett. 7 (2007) 2645.
[39] C. Suryanarayana, E. Ivanov, V.V. Boldyrev, Mater. Sci. Eng. A 304–306 (2001) 151.
[40] R. Pérez-Bustamante, F. Pérez-Bustamante, I. Estrada-Guel, L. Licea-Jiménez, M. Miki-Yoshida, R. Martínez-Sánchez, Mater. Charact. 75 (2013) 13.
[41] B.I. Yakobson, Appl. Phys. Lett. 72 (1998) 918.
[42] K. Min, N.R. Aluru, Appl. Phys. Lett. (2011) 98.
[43] J.B. Nelson, D.P. Riley, Proc. Phys. Soc. 57 (1945) 477.
[44] A.J. Trowsdale, B. Noble, S.J. Harris, I.S.R. Gibbins, G.E. Thompson, G.C. Wood, Corros. Sci. 38 (1996) 177.
[45] E.M. Sherif, A.A. Almajid, F.H. Latif, H. Junaedi, Int. J. Electrochem. Sci. 6 (2011) 1085.
[46] M. Saxena, O.P. Modi, A.H. Yegneswaran, P.K. Rohatgi, Corros. Sci. 27 (1987) 249.
[47] T.-C. Yeh, T.-C. Huang, H.-Y. Huang, Y.-P. Huang, Y.-T. Cai, S.-T. Lin, Y. Wei, J.-M. Yeh, Polym. Chem. 3 (2012) 2209.
[48] E.M. Sherif, S.-M. Park, J. Electrochem. Soc. 152 (2005) B205.
[49] E.M. Sherif, S.-M. Park, Electrochim. Acta 51 (2006) 1313.
[50] N. Sato, Corros. Sci. 37 (1995) 1947.
[51] F. Hunkeler GSF, H. Bohni, Corros. (Houston) 43 (1987) 189.
[52] L. Tomcsányi, K. Varga, I. Bartik, H. Horányi, E. Maleczki, Electrochim. Acta 34 (1989) 855.
[53] Y. Kim, J. Lee, M.S. Yeom, J.W. Shin, H. Kim, Y. Cui, J.W. Kysar, J. Home, Y. Jung, S. Jeon, Nat. Commnun. 4 (2013) 1.
[54] T.W. Clyne, An Introduction to Metal Matrix Composites. An Introduction to Metal Matrix Composites, Cambridge University Press, Cambridge, 1995, p. 26.
[55] R.M. Aikin Jr, L. Christodoulou, Scr. Metall. Mater. 25 (1991) 9.
[56] K. Chu, Z. Liu, C. Jia, H. Chen, X. Liang, W. Gao, W. Tian, H. Guo, J. Alloy. Compd. 490 (2010) 453.
[57] A. Yu, P. Ramesh, M.E. Itkis, E. Bekyarova, R.C. Haddon, J. Phys. Chem. C 111 (2007) 7565.
[58] M. Estili, A. Kawasaki, Y. Sakka, Adv. Mater. 24 (2012) 4322.
[59] X. Wang, C. Zhi, L. Li, H. Zeng, C. Li, M. Mitome, D. Golberg, Y. Bando, Adv. Mater. 23 (2011) 4072.
[60] M. Rashad, F. Pan, M. Asif, S. Hussain, M. Saleem, Mater. Charact. 95 (2014) 140.
[61] M. Rashad, F. Pan, A. Tang, M. Asif, J. Ind. Eng. Chem. 20 (2014) 4250.
[62] M. Rashad, F. Pan, M. Asif, A. Ullah, Mater. Sci. Technol. 31 (2015) 1452.
[63] M. Rashad, F. Pan, H. Hu, M. Asif, S. Hussain, J. She, Mater. Sci. Eng.: A 630 (2015) 36.